

SCIENTIFIC REPORTS



OPEN

Mechanical milling: a sustainable route to induce structural transformations in MoS₂ for applications in the treatment of contaminated water

Maria Cantarella¹, Giuliana Gorrasi², Alessandro Di Mauro¹, Mario Scuderi³, Giuseppe Nicotra³, Roberto Fiorenza⁴, Salvatore Scirè⁴, Maria Elena Scalisi⁵, Maria Violetta Brundo⁵, Vittorio Privitera¹ & Giuliana Impellizzeri¹

Two-dimensional (2D) nanomaterials have received much attention in recent years, because of their unusual properties associated with their ultra-thin thickness and 2D morphology. Besides graphene, a new 2D material, molybdenum disulfide (MoS₂), has attracted immense interest in various applications. On the other hand, ball-milling process provides an original strategy to modify materials at the nanometer scale. This methodology represents a smart solution for the fabrication of MoS₂ nanopowders extremely-efficient in adsorbing water contaminants in aqueous solution. This work reports a comprehensive morphological, structural, and physicochemical investigation of MoS₂ nanopowders treated with dry ball-milling. The adsorption performances of the produced nanopowders were tested using methylene blue (MB) dye and phenol in aqueous solution. The adsorption capacity as a function of ball-milling time was deeply studied and explained. Importantly, the ball-milled MoS₂ nanopowders can be easily and efficiently regenerated without compromising their adsorption capacity, so to be reusable for dye adsorption. The eventual toxic effects of the prepared materials on microcrustacean *Artemia salina* were also studied. The present results demonstrate that ball-milling of MoS₂ offers a valid method for large-scale production of extremely efficient adsorbent for the decontamination of wastewaters from several pollutants.

Stimulated by the numerous studies devoted to exploit the extraordinary properties of graphene, recently, other two-dimensional (2D) materials are attracting a lot of attention. Among the 2D materials, emerging transition metal dichalcogenides and in particular, molybdenum disulfide (MoS₂), have received enormous interest because of its unique structural, thermal, mechanical and electronic properties¹. MoS₂ possesses a layered structure consisting of layers of S-Mo-S, where a Mo atom layer is sandwiched by two layers of S atoms. Crystals of MoS₂ are composed of vertically stacked layers held together by relatively weak van der Waals interactions in a hexagonally-packed structure. MoS₂ is a semiconductor with an indirect band-gap of ~1.2 eV in multilayer structure that turns into a direct band-gap of ~1.9 eV upon processing to a single layer². Furthermore, MoS₂ has a good chemical stability and remains stable in acids, alkalis and organic solvents³⁻⁵. Thanks to its properties MoS₂ in a few years imposed itself as an attractive material for several applications, such as for electronic transistors, lubrication, catalysis, energy storage, sensors, photodetectors, etc^{1,6}. Recently, many studies are also directed to the use of MoS₂ nanostructures for water treatment applications⁷⁻⁹.

Water purification is still one of the most serious problem in the world. Indeed, augmented agricultural and industrial activity has produced an increased contamination of our limited water resources due to the dispersion

¹CNR-IMM, Via S. Sofia 64, 95123, Catania, Italy. ²Department of Industrial Engineering, University of Salerno, Via Giovanni Paolo II 132, 84084, Fisciano, Salerno, Italy. ³CNR-IMM, Z.I. VIII Strada 5, 95121, Catania, Italy. ⁴Department of Chemical Sciences, University of Catania, Viale Andrea Doria 6, 95125, Catania, Italy. ⁵Department of Biological, Geological and Environmental Sciences, University of Catania, Via Androne 81, 95124, Catania, Italy. Correspondence and requests for materials should be addressed to M.C. (email: maria.cantarella@ct.infn.it)

of various organic pollutants, such as industrial dyes, aromatic compounds, and heavy metal ions¹⁰. Consequently, numerous efforts are emerged to develop cheap and efficient technologies for water treatment, able to guarantee abundant clean water and create environmental and public health sustainability^{11–18}. Currently, adsorption of pollutants through activated carbon is one of the most popular method for water treatment due to its effectiveness. However, commercial activated carbon is relative expensive due to the high production cost, high regeneration cost that requires high-pressure stream, and 10–15% loss in the reactivation procedure^{19,20}.

Nanostructured MoS₂ can be a valid alternative to the conventional materials for water treatment²¹. Some researchers have focused their attention to the use of MoS₂ nanosheets as photocatalyst for the degradation of organic pollutants and bacteria inactivation^{7,22,23}. As mentioned before, single layers of MoS₂ are characterized by band-gap values that make MoS₂ a potential visible-light photocatalyst. Charge carriers are generated in the valence and conduction bands under visible light irradiation. However, the recombination rate of the photo-generated electron-hole pairs is extremely high making smaller the photocatalytic efficiency. To reduce this phenomenon, the realization of nanocomposites with large band-gap metal oxide in which MoS₂ is used as co-catalyst is inevitable to really degrade the contaminants through a photocatalytic mechanism^{24–28}. Another interesting feature of MoS₂ is the capacity to act as a very efficient adsorbent for organic molecules. The source of these adsorption abilities is due to the stacked planar structure of MoS₂. The adjacent planes of MoS₂, held together by van der Waals interactions, allow molecules or atoms to infiltrate and diffuse freely between the layers where they adsorb²⁹. This extraordinary property of MoS₂ has not been exploited extensively, despite the adsorption process through nanostructured materials is considered an efficient and economical method for the removal of contaminants from water at large-scale^{30,31}. To date, only few examples are present in the literature in which MoS₂ is efficiently used as adsorbent for water treatment, and they involve the realization of sophisticated nanostructures or the functionalization of MoS₂ surface in order to increase the number of adsorption sites^{32–46}.

In this work, we treated commercial MoS₂ nanopowders with a dry ball-milling process. We demonstrated that this simple and highly-scalable method⁴⁷ can significantly enhance the adsorption properties of the MoS₂ without the need of any additional reaction or involvement of chemical agents. Some examples of ball-milling process applied to MoS₂ to exfoliate bulk MoS₂^{48–50} or to modify the electrochemical and catalytic properties^{51–53} have been already reported in the literature. However, to our knowledge, there are not studies focused on the application of ball-milling to produce efficient MoS₂ adsorbents. The ball-milled materials were deeply characterized by scanning electron microscopy (SEM), N₂ adsorption-desorption measurements, transmission electron microscopy (TEM), X-ray diffraction (XRD) analyses, and X-ray photoelectron spectroscopy (XPS). The adsorption capacity was tested using methylene blue (MB) dye and phenol as representative water pollutants. In addition, potential toxic effects of the MoS₂ nanopowders on microcrustacean *Artemia salina* were originally evaluated.

Methods

Materials. Commercial molybdenum disulfide nanopowders (MoS₂), with a theoretical diameter of 90 nm (99% trace metal basis) were purchased from Sigma-Aldrich and hereafter simply called “as received”.

Methylene Blue (MB, 0.05 wt% in H₂O) and phenol (C₆H₅OH, ≥99.5%) were also purchased from Sigma-Aldrich.

Ball-Milling procedure. As received MoS₂ powders (3 g) were milled in a planetary ball milling PM100 (Retsch) at ambient temperature. The jar volume was 50 cm³, the used balls (5) were of tungsten carbide, the milling rate equal to 450 rpm and the milling time up to 40 h. The machine was interrupted every 4 hours and the material mixed up with a tongue.

Characterization methods. SEM analyses were performed with a field emission Zeiss Supra 25 microscope operating at 5 kV.

The N₂ adsorption-desorption experiments were carried out in a Sorptomatic 1990 Micropore configuration (Thermo Quest). Before tests, the samples were degassed at 120 °C at 10^{−3} Torr. The physisorption experiments were performed at liquid nitrogen boiling temperature (77 K). Surface area and pore size distribution were evaluated with the help of a fully computerized unit attached to the Micropore unit system, using the Brunauer-Emmett-Teller (BET) equation and the Dollimore-Heal method, respectively.

The nanoscale morphological and structural characterization of MoS₂ nanopowders was carried out by TEM. The analyses were performed with a Cs-probe-corrected JEOL JEM ARM200CF microscope at primary beam energy of 200 keV operated in scanning TEM (S/TEM) mode. As for the specimen preparation, the powders were dispersed in isopropyl alcohol by sonication for 15 min, thereafter 5 μL of each dispersion were deposited on an Au TEM grid with a lacey carbon support film. In order to obtain images of MoS₂ nanopowders with Z-contrast, the high-angle annular dark field mode (HAADF) was used with a convergence semi-angle of 33 mrad and a collection semi-angle in a range comprised between 64 mrad and 172 mrad.

XRD patterns of MoS₂ nanoparticles were detected by a Bruker D-500 diffractometer at 40 kV and 40 mA, using a Cu Kα line of 0.15418 nm wavelength. The angle of incidence was fixed at 2.5°, and the diffractogram was collected from 10 to 60°. The XRD patterns were analyzed by the Bruker software suite, including ICSD structure database.

XPS measurements were performed by a PHI ESCA/SAM 5600 Multy technique spectrometer with the use of a Mg standard X-ray source. The pressure in the chamber was ~10^{−9} Torr. The analyses were carried out at 45° photoelectron takeoff angle relative to the sample surface with an acceptance angle of ±3°. The analyzer pass energy was set at 23.5 eV for the high resolution of all the spectra in the regions of C 1s, O 1s, Mo 3d and S 2p. The binding energy (BE) scale was calibrated by centering the C 1s signal of the aliphatic/aromatic component at 285.0 eV.

Adsorption test. The adsorption properties of as received and ball-milled MoS₂ nanopowders were examined through the adsorption of MB dye and phenol in aqueous solutions. In a typical experiment, 1.4 mg of MoS₂ nanopowders were added in 2 mL of MB solution with a starting concentration of 1.5×10^{-5} M (4.8 ppm), at room temperature and with a pH of ~ 7.5 . The test was run in parallel for each type of MoS₂ nanopowders. At regular time intervals, the solutions were collected and centrifuged at 13000 rpm for 10 min, so to separate the nanopowders. In order to evaluate the adsorption of MB onto MoS₂, the variation in the dye concentration was evaluated spectrophotometrically (using a PerkinElmer Lambda 45 UV-vis spectrophotometer) via the solution absorbance at 664 nm in the Lambert-Beer regime⁵⁴. The dye adsorption on the beaker walls was also checked, as a reference, in the absence of the nanopowders. Every 20 min, the solutions were replaced with fresh MB solutions and the adsorption cycle was repeated with the same procedure. After three cycles, the MoS₂ nanopowders were washed with NaOH 0.1 M for a few minutes, in order to restore the adsorption properties of the MoS₂.

The aptitude of the investigated MoS₂ nanopowders to adsorb phenol in aqueous solution was also tested, by measuring (using a Hach DR 3900 spectrophotometer) the residual concentration of phenol solution after 20 min of staying in contact with the nanopowders. 1.4 mg of MoS₂ nanopowders were added in 2 mL of phenol solution (starting concentration of phenol: 1.5×10^{-5} M) at room temperature. Also in this case, before to perform the measure the powders were separated from the solutions by centrifuging them at 1300 rpm for 10 min. A blank experiment was done in parallel as control.

Artemia salina acute toxicity test. Commercially available *Artemia salina* dehydrated cysts were purchased from local aquarium store (ArtemiaCyst Blue Line, Italy). Cysts were first hydrated in ASPM seawater solution (ASPM is a synthetic seawater made of: NaCl = 26.4 g, KCl = 0.84 g, CaCl₂·H₂O = 1.67 g, MgCl₂·H₂O = 4.6 g, MgSO₄·7H₂O = 5.58 g, NaHCO₃ = 0.17 g and H₃BO₃ = 0.03 g) and then washed to separate the floating cysts (i.e., dead) from those that sink (i.e. alive). The sinking cysts were collected, and approximately 1 g of the pre-cleaned cysts were incubated in 800 mL of ASPM solution seawater in a conical plastic container with graduations. A 1.500 lux daylight was provided continuously by a fluorescent lamp. Aeration was maintained by a small line extending to the bottom of the hatching device from an aquarium air pump. Under conditions of incubation at room temperature (26 ± 1 °C), gentle aeration and continuous illuminations, the nauplii hatched within 24 h. Two stock solutions of as received MoS₂ (5 mg/mL) and ball-milled MoS₂ 40 h (5 mg/mL) after dilution in ASPM solution, were prepared. Then, fresh suspensions with different concentrations of nanopowders (10^{-1} and 10^{-2} mg/mL) were made starting from the stock suspensions. These solutions were vortexed for 30 seconds, and then sonicated in an ultrasonic bath for about 20 minutes. 200 μ L of each different concentrations of nanopowders solutions were added to the 96-well microplates. After that, 1 nauplius per well was added and incubated at 26 °C for 24/48 hours. The number of surviving nauplii in each well was counted under a stereomicroscope after 24/48 hours. A control group was also setup with ASPM seawater solution only. Larvae were not fed during the bioassays. The endpoint (immobility, i.e. death) was assessed at the end of the test by a stereomicroscope (a Leica EZ4): a nauplius was considered to be immobile or dead, if it could not move its antennae after slight agitation of the water for 10 seconds. Larvae that were completely motionless were counted as dead, and the percentages of mortality compared to the control were calculated. The death % of the crustacean for each concentration was calculated as follow: (n. dead nauplii/n. total animal treated) • 100. The collected data were analyzed for significance by one-way ANOVA test.

Results and Discussion

The ball-milling process was applied to commercial MoS₂ nanopowders, for 20 or 40 hours, in order to evaluate the effect of the process on the adsorption properties of the MoS₂.

SEM, in plan-view, was used to investigate the morphological alterations induced by the milling process. Figure 1a shows a SEM image of the MoS₂ nanopowders before the ball-milling. Large MoS₂ flakes (about 1 μ m in size) together with little flakes (about 100 nm in size) can be seen. Figure 1b,c clearly evidence rounded flakes in comparison with the as received materials (Fig. 1a) as a result of the ball-milling process. Besides this evident difference between the as received and ball-milled nanopowders, SEM images do not show any other diversity, nor do reveal any variation in the size of the nanopowders, within the SEM resolution of course.

Consequently, in order to investigate an eventual reduction in size of the as-received MoS₂ nanopowders thanks to the ball-milling process, the textural properties of the samples were measured through the BET and the Dollimore-Heal methods. In Table 1 the obtained specific surface area, pore specific volume and mean pore diameter values for the three different samples are reported. These results reveal an increase of the specific surface area after the ball-milling process. In particular, the increase of surface area is $\sim 27\%$ after 20 hours of ball-milling and $\sim 42\%$ after 40 hours of ball-milling compared to the obtained values for the as received nanopowders. As a consequence of the ball-milling process, a decrease of mean pores diameter and of pores volume was also detected if compared to the as received material, with the formation of micropores included in the 1–2 nm range for the 20 and 40 hours ball-milled materials, that are absent in the as received sample as reported in the Fig. 2.

In Fig. 3 we show the results of TEM analyses for the as received MoS₂ flakes (a-c-e) and the ones exposed to 40 hours of ball-milling (b-d-f), respectively. The S/TEM Z-contrast images, obtained before the ball-milling process, show the MoS₂ flakes having a flat shape (Fig. 3a), in particular the specimen looks to be formed of nano flakes with different area and shape stacked on top of each other. They assume a more rounded shape after the ball-milling exposure (Fig. 3b), and appear to be very crumpled, where randomly two different type of structures could be recognized. A first type of structure is reported to be as amorphous and porous-like. This kind of structure is usually present on a contaminated specimen by hydrocarbon components, which usually experiences the formation of voids, due to his sublimation under electron beam irradiation by TEM⁵⁵. A second type of structures shows a number of random oriented bright stripes (arrows in Fig. 3b). In this case MoS₂ lattice planes are compacted and randomly oriented due to ball-milling exposition, and differently by the as received specimen, where

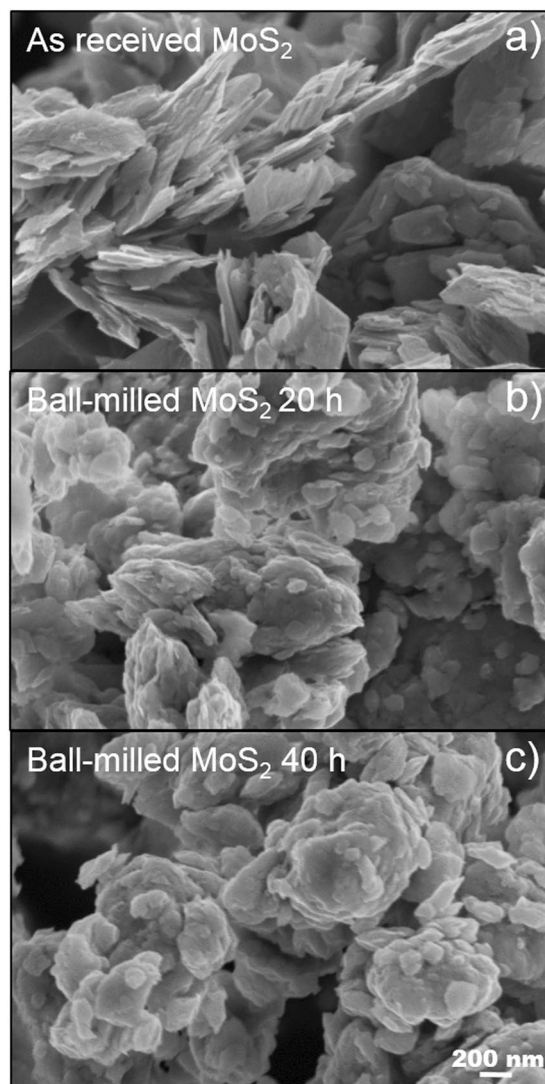


Figure 1. SEM images of as received MoS₂ (a), ball-milled MoS₂ for 20 hours (b), and ball-milled MoS₂ for 40 hours.

	Specific Surface Area	Pore Specific Volume	Mean Pore Diameter
As received MoS ₂	26 ± 1 m ² /g	0.09 ± 0.02 cm ³ /g	11.2 ± 0.1 nm
Ball-milled MoS ₂ 20 h	33 ± 1 m ² /g	0.06 ± 0.02 cm ³ /g	7.8 ± 0.1 nm
Ball-milled MoS ₂ 40 h	37 ± 1 m ² /g	0.04 ± 0.02 cm ³ /g	6.9 ± 0.1 nm

Table 1. Specific surface area, pore specific volume and mean pore diameter values, of the as received MoS₂ and the ball-milled MoS₂ for 20 hours and 40 hours.

the lattice planes perfectly stacked and easy to be aligned with the electron beam of the TEM, here only the lattice planes accidentally aligned with the electron beam show a brighter contrast, while the others give an uniform contrast as background.

The high-resolution image in Fig. 3c and his relative fast Fourier transform (FFT), taken on a portion of the as received specimen, (see red square in Fig. 3a), shows the regular crystalline nature of the MoS₂. In particular, the FFT shows two pattern corresponding to the P63/mmc space group⁵⁴ aligned on the (001) zone axis. This means that two coplanar flakes are rotated by few degrees one other, around the a-axis. In Fig. 3e, HAADF Z-contrast STEM at higher magnification shows the direct atomic structure of the MoS₂ crystal lattice that is the same as the one predicted by the theoretical reconstruction reported into the inset⁵⁶. The absence of contrast modulation on the Z-contrast image in correspondence of the heavy Mo, compared with the light S atoms, implies the presence of AB stacking of MoS₂ lattice planes, i.e. atoms of Mo and S are regularly alternated each other, along the same atomic column.

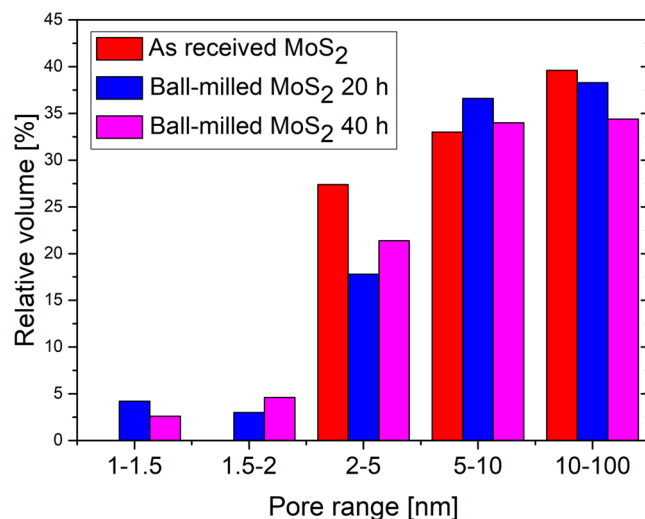


Figure 2. Pore size distribution for the as received MoS₂ and the ball-milled MoS₂ for 20 hours and 40 hours, respectively.

The presence of a regular atomic structure, as reported on the high-resolution S/TEM image of Fig. 3d, taken at a portion of the ball-milled flake evidenced by the red square in Fig. 3b, confirms the persistence of its crystalline nature. The in-plane view at this region permits to put in evidence the MoS₂ layers stacked up along the c-axis. Due to the weak van der Waals forces, these layers, after the milling exposure, change their original distance between planes that is then not constantly maintained. In Fig. 3f a comparison between the real crystal structure from a non-damaged area and his theoretically reconstructed crystal structure⁵⁶ is illustrated. The measured inter-planar distance of 6.15 Å is in good agreement with the one reported in the literature for MoS₂⁵⁷.

Summarizing the results of the TEM analysis, the ball-milling process modifies the overall structure order of the flakes. They go from a perfectly flat stacked crystalline structure to a round shaped one made by crumpled but still crystalline planes of MoS₂. The thickness of the MoS₂ flakes has been estimated by TEM analyses and resulted to be 5–6 nm.

Figure 4 shows the XRD patterns of the as received MoS₂ nanopowders (red line) and of the samples ball-milled for 20 hours (blue line) or 40 hours (magenta line). The spectrum of the as received sample shows all the reflections of molybdenite, as reported in JCPDS cards no. 37–1492: the (100), (103) and (110) reflections could be readily indexed as hexagonal MoS₂^{58,59}. Even if the crystallinity is maintained after the aggressive process of ball-milling, a decrease of all the peaks with the increase of the ball-milling time, is evident. In particular, the peak at 14.4° related to the (002) reflection⁵⁷, associated with the sheet of MoS₂, has a maximum intensity in the as received sample but gradually disappears with the ball-milling process, indicating that the MoS₂ layers are not yet orderly stacked but splitted apart.

XPS measurements were performed before and after the ball-milling for 40 hours, in order to investigate the surface chemical composition of the nanopowders. From the survey spectra of both samples (not reported here) the signals of O, C, Mo, and S were detected, so demonstrating that no contaminant is present neither in as received nanopowders nor in ball-milled powders (within the XPS resolution). In the well-resolved Mo 3d spectrum (Fig. 5a) of the as received sample, two peaks at 229.3 eV (Mo 3d_{5/2}) and 232.4 eV (Mo 3d_{3/2}) were observed and attributed to the Mo⁴⁺ oxidation state of MoS₂. In the S 2p spectrum for the same sample (Fig. 5b), the peaks at 162.0 eV and 163.5 eV, attributed to S 2p_{3/2} and S 2p_{1/2} respectively, are associated with the divalent S in the MoS₂. The same characteristic peaks were observed also for the samples submitted to ball-milling (Fig. 5d,e); the only difference is the presence of a bump in both Mo and S spectrum (peaked at ~236 eV and ~169 eV, respectively). This bump is probably due to a surface oxidation. The amount of oxidation was calculated by comparing the area of the peaks of oxidized species at 236 eV and at 169 eV with the totally area of Mo and S peaks, respectively. The results of this exercise gave an increase of 20% of oxidation in both regions. This result can be ascribed to the higher exposed surface area of the ball-milled material (as demonstrated by BET measurements). In order to investigate the eventual presence of new oxidative species induced by the ball-milling process, the oxygen regions are reported for both samples in Fig. 5c,f; this analysis does not show any other species.

The adsorbance capacity of the investigated MoS₂ nanopowders was tested through the adsorption of MB dye in aqueous solution. The obtained results are presented in Fig. 6, where the variation in the MB concentration as a function of the time is reported. The test was run in parallel for the as received MoS₂ nanopowders (Fig. 6a), ball-milled MoS₂ for 20 hours (Fig. 6b), and ball-milled MoS₂ for 40 hours (Fig. 6c). In order to exclude any possible effects due to the adsorption of the organic dye on the beaker walls, the variation in the MB concentration in the absence of any adsorbent was also checked as reference and plotted as a black line in each graph. The color of the blue dye starts to fade in the presence of MoS₂, thus suggesting the removal of the dye from water by its adsorption onto the surface of the nanopowders. In the first cycle, the solutions were collected after 10 min, centrifuged and measured using a spectrophotometer. The procedure was repeated after other 10 min. The adsorption

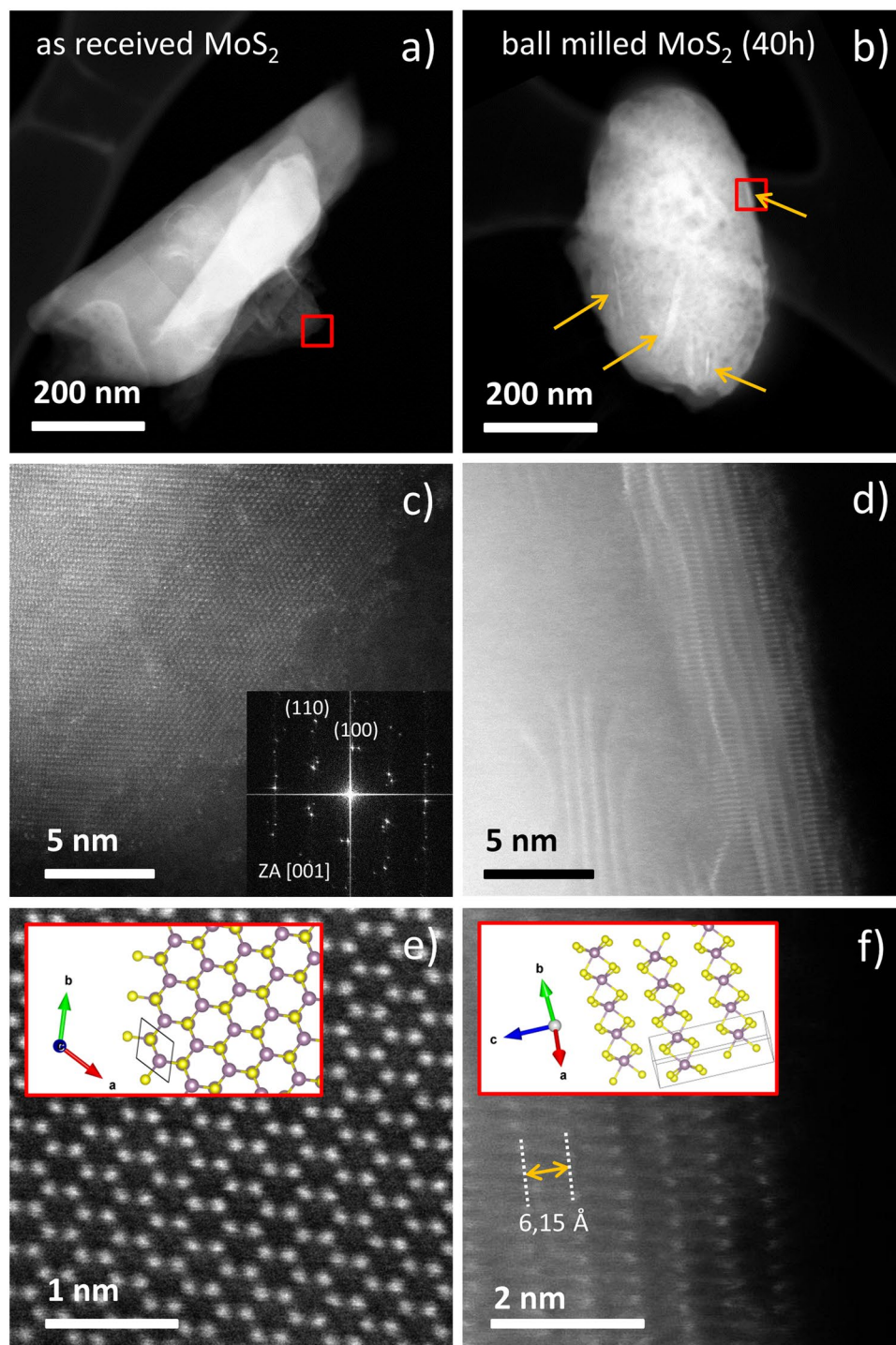


Figure 3. HAADF Z-contrast S/TEM images of as received MoS₂ (a-c-e), and ball-milled for 40 hours (b-d-f). Low magnification of a single flaker of as received MoS₂ (a); atomically resolved Z-contrast S/TEM image of the region indicated by a square in Figure 3a and his relative FFT (inset) (c); high magnification of the atomically resolved Z-contrast S/TEM image of Figure 3c with the simulated crystal structure (e). Low magnification of a single ball-milled flake (b); atomically resolved Z-contrast S/TEM image of the region indicated by a square in Figure 3b (d); high magnification of the atomically resolved Z-contrast S/TEM image of Figure 3d clearly showing the direct crystal-line structure (f).

of MB on the as received MoS₂ was ~30% after 20 min (Fig. 6a). In the same time frame, ball-milled powders for 20 hours were able to adsorb ~80% of the dye (Fig. 6b). More interestingly, MB adsorption on ball-milled MoS₂ nanopowders for 40 hours was found to be very fast and 100% of the dye was removed from water within only 20 min (Fig. 6c). Every 20 min the solutions were replaced with fresh MB solutions (this change is marked in the

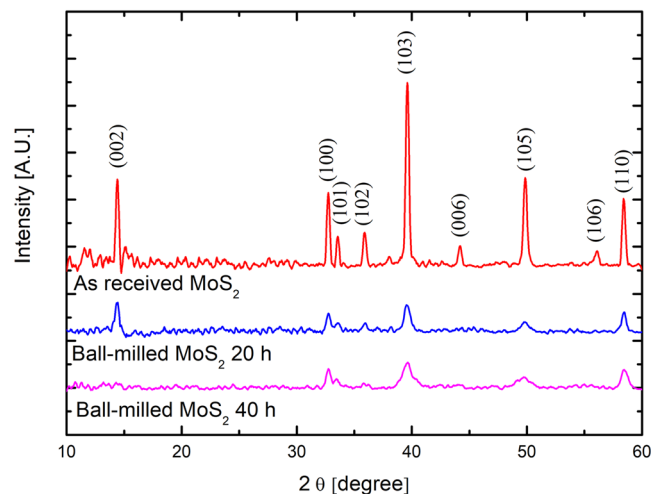


Figure 4. XRD pattern for as received MoS₂, ball-milled MoS₂ for 20 hours, and ball-milled MoS₂ for 40 hours.

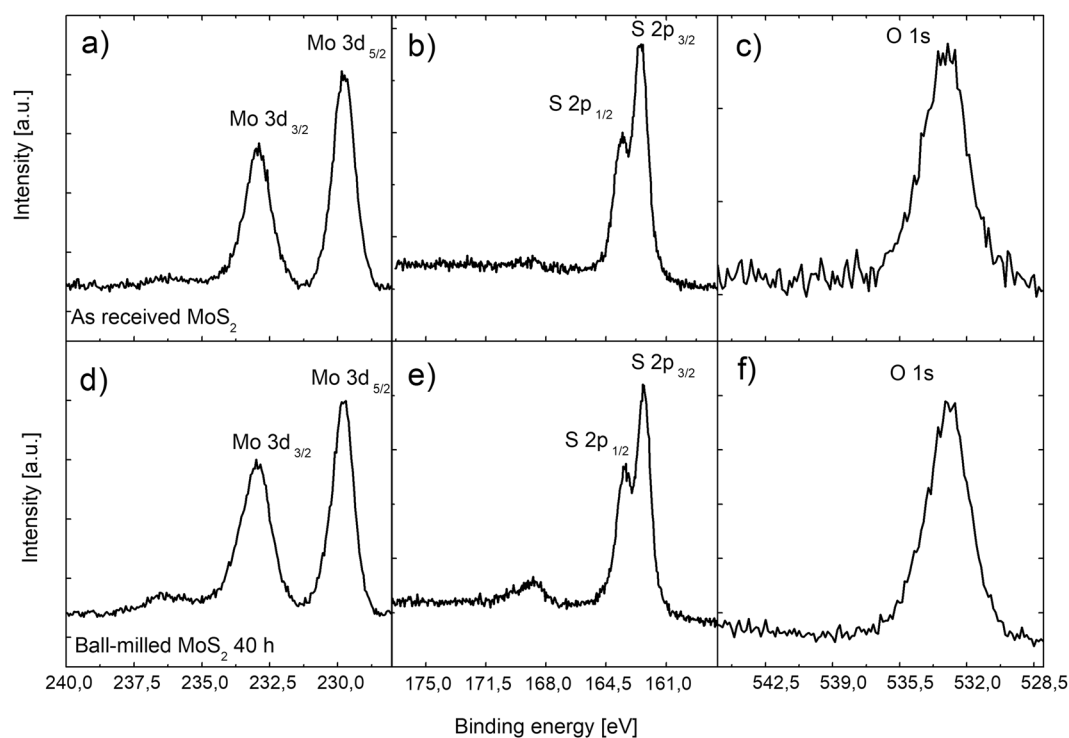


Figure 5. Mo 3d (a), S 2p (b) and O 1s (c) spectra for the as received MoS₂; Mo 3d (d), S 2p (e) and O 1s (f) spectra for the ball-milled MoS₂ for 40 hours.

graphs with vertical dashed lines), and the adsorption cycles were repeated with the same procedure reported above. During the second cycle, the as received MoS₂ removed less than 5% of MB, ball-milled MoS₂ for 20 hours and 40 hours removed ~40% and ~80% of the dye, respectively. During the third cycle, the as received MoS₂ continued to adsorb less than 5% of MB, ball-milled samples for 20 hours and 40 hours removed almost 40% and 70% of the dye, respectively. Since the adsorption process is a surface-driven process, the reduction of the adsorption capacity for all the samples is surely due to a reduction of the available sites for the physisorption process on the surface of the samples. With the main aim of reactivating the surface of the samples, and verify their reusability, the MB adsorbed on the nanopowders was removed by washing them for a few minutes with an aqueous solution of sodium hydroxide (the washing is marked with a vertical solid line in Fig. 6). We found that all tested samples recovered their starting adsorption performances, so demonstrating that the MoS₂ could be easily recycled and consequently reused without any degradation of the adsorption sites. The little differences in the adsorption efficiency, if compared with the efficiency at the beginning of the test (for example, for the ball-milled MoS₂

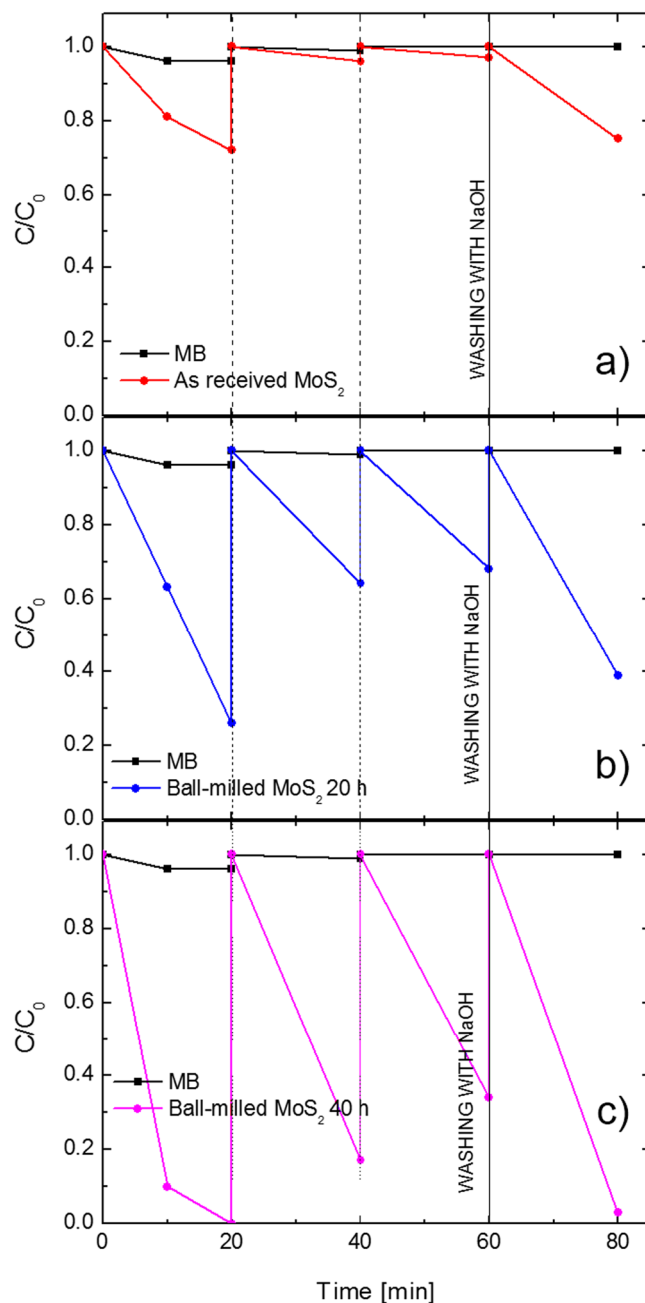


Figure 6. MB adsorption onto the as received MoS₂ (a), ball-milled MoS₂ for 20 hours (b), and ball-milled MoS₂ for 40 hours (c). Vertical dashed lines indicate the change of the MB solution. Vertical solid line indicates the nanopowders washing step. The oblique lines are guide for eyes.

nanopowders for 40 hours the adsorbance efficiency changes from 100% to 97%), is due to a small loss of nanopowders during the centrifugation steps.

We deeply investigated the adsorption kinetic and the adsorption capacity at the equilibrium of the ball-milled nanopowders. Adsorption tests were performed using 10 mL of aqueous solution with a MB concentration of 100 ppm. 7 mg of ball-milled MoS₂ for 40 hours was used as adsorbent and added to the MB solution. Under these experimental conditions, the system is able to reach the equilibrium point, i.e. the point in which the dye adsorbed is equal to the dye desorbed by the adsorbent, so that the concentration of the dye in the solution remains constant. At regular time intervals, aliquots of the dispersion were collected and after dilution, the concentration of MB dye was examined spectrophotometrically until reaching the equilibrium point. The obtained results are reported in Fig. 7a. The adsorption capacity at the equilibrium, Q_e (mg g⁻¹), was calculated by using the following equation:

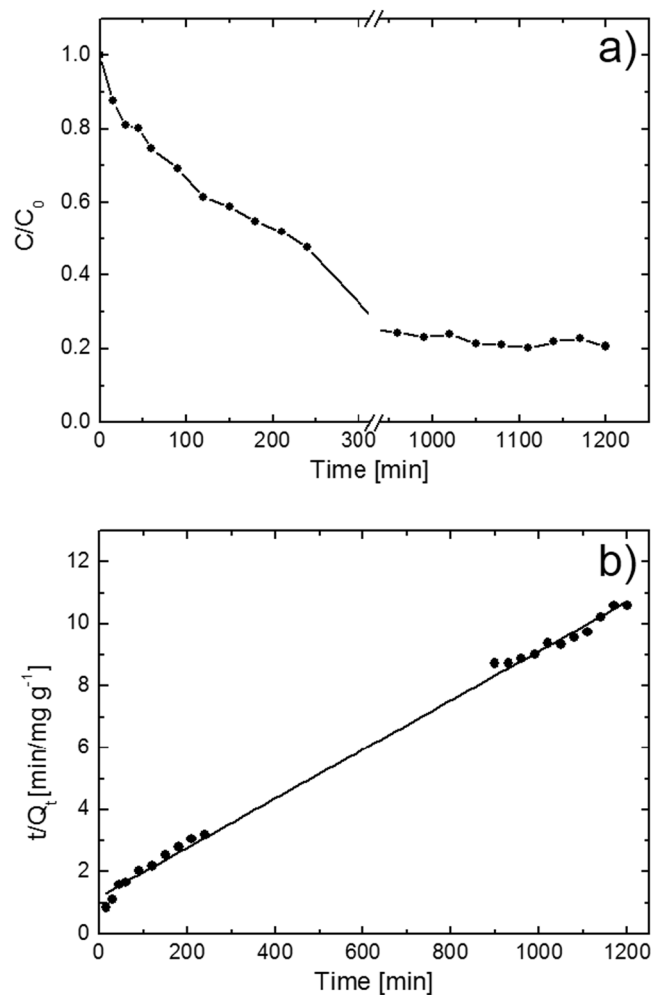


Figure 7. MB adsorption onto the ball-milled MoS₂ for 40 hours (a) (the line is guide for eye); adsorption kinetic of MB onto the ball-milled MoS₂ for 40 hours compared with the pseudo-second-order model (b).

$$Q_e = (C_0 - C_e) \times V/W \quad (1)$$

where, C_0 (mg L⁻¹) is the initial concentration of MB, C_e (mg L⁻¹) is the concentration of MB at the equilibrium, V (L) is the volume of wastewater, W (g) is the amount of MoS₂ used as adsorbent. At the equilibrium, the ball-milled MoS₂ for 40 hours nanopowders have an adsorption capacity of ~113 mg g⁻¹. This value is significantly higher of the adsorption capacity for many examples of MB adsorbent described in the literature^{60–63}.

In the present study, linear pseudo-first-order (eq. 2), linear pseudo-second-order (eq. 3), and intraparticle diffusion (eq. 4) adsorption models were used to fit our experimental data. The models are expressed, respectively, by the following equations^{64–66}:

$$\ln(Q_e - Q_t) = \ln Q_e - k_1 t \quad (2)$$

where Q_t (mg g⁻¹) is the amount of dye adsorbed at time t (min), k_1 is the pseudo-first-order rate constant (min⁻¹).

$$\frac{t}{Q_t} = \frac{1}{k_2 Q_e^2} + \frac{t}{Q_e} \quad (3)$$

where k_2 is the pseudo-second-order rate constant (g mg⁻¹ min⁻¹).

$$Q_t = k_{id} t^{0.5} + C \quad (4)$$

where k_{id} is the intraparticle diffusion rate constant (mg g⁻¹ min^{-1/2}).

Based on these three models, curve fitting were performed. We found that our experimental data fit more closely to the pseudo-second-order model with R^2 of 0.997 (Fig. 7b). Instead, for the pseudo-first-order and intraparticle diffusion models the R^2 values are 0.834 and 0.967, respectively, revealing that these two models are not suitable to describe our adsorption process.

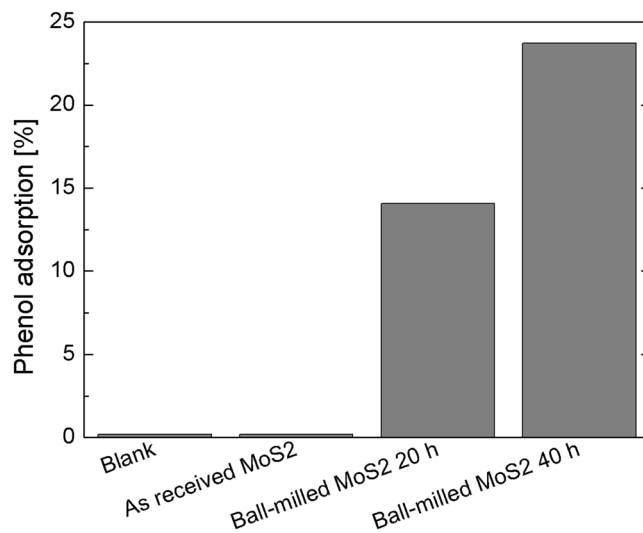


Figure 8. Phenol adsorption onto as received MoS₂, ball-milled MoS₂ for 20 or 40 hours.

The extremely high adsorption of ball-milled MoS₂ was further tested for the adsorption of phenol, a toxic and water refractory pollutant, widely used in many industrial processes but hardly removed through common wastewater treatment methods⁶⁷. After 20 min the solution was collected and centrifuged, while the residual phenol concentration was measured using a spectrophotometer. Figure 8 reports the percentage of adsorbed phenol by each sample, compared to a blank experiment, i.e. a phenol solution without nanopowders. The data clearly illustrates that the as received MoS₂ nanopowders are not able to remove phenol at all. On the contrary, MoS₂ nanopowders submitted to ball milling process for 20 and 40 hours are able to adsorb ~15% and ~25% of phenol, respectively, in only 20 min.

As it was done for MB adsorption, the adsorption kinetic and the adsorption capacity at the equilibrium for phenol was deeply investigated. The experiment was performed using 10 mL of aqueous solution of phenol 100 ppm in which 7 mg of ball-milled MoS₂ for 40 hours were added. At regular time intervals, aliquots of the dispersion were collected and after dilution, the concentration of phenol was examined spectrophotometrically until reaching the equilibrium point. The obtained results are reported in the Fig. 9a. The adsorption capacity at the equilibrium was calculated by using eq. 1 and it resulted 63 mg/g, confirming the lower affinity of MoS₂ towards phenol. Also in this case the experimental data fit more closely to the pseudo-second-order model (see Fig. 9b) with R² of 0.996.

Figure 10 shows on the left vertical axis the % removal efficiency for MB dye and phenol as a function of the milling time. A linear trend can be easily detected for both contaminants; in particular the experimental data for MB can be fitted by the following straight line: %MB ads = 31 + 1.8 t, while the data for phenol can be fitted by the following straight line: %phenol ads = 0.91 + 0.59 t, where t is here the milling time. A higher efficiency in the adsorbance of MB compared to phenol can be clearly evidenced already for the as received samples. The lower efficiency in adsorbing phenol with respect to MB dye can be explained with an electrostatic repulsion between the negative charge density typical of the aromatic ring of the phenol and negative charge density on the sulfur atoms present in the MoS₂ surface. On the contrary, the adsorption of MB is favorite thanks to the positive charge present in the MB molecule. Figure 10 also reports on the right vertical axis the specific surface area increment as a function of the milling time as obtained by BET measurements. The data can be fitted by the following straight line: %surf. area = 0.89 + 1.09 t. The observed correlation between the adsorption trend and the specific surface area trend clearly indicates that the adsorption efficiency strongly depends on the exposed surface area of the nanopowders. Higher exposed surface area means higher number of adsorption sites, and thus higher efficiency in the adsorbance of water contaminants. The error in the evaluation of both adsorption efficiency and specific surface area increment is within the symbol where it does not appear in the graph.

Finally, the potential toxicity of the as received and ball-milled MoS₂ nanopowders was originally evaluated by testing the effects of the materials on microcrustacean *Artemia salina* in aquatic environment. *Artemia* is a non-selective filter-feeder organism that can readily ingest fine particles smaller than 50 μm⁶⁸. For this reason, it is a model organism in toxicity assessment of nanoparticles. The accumulation of the nanomaterials into the *Artemia salina* was evaluated qualitatively at the end of the exposure (24 and 48 hours) thanks to a stereomicroscope equipped with a digital camera. After 24 hours, compared with the controls (Fig. 11a), the guts of the exposed larvae to MoS₂ nanopowders were filled with particles (Fig. 11b,c). The ingested particles appeared as a long strip of particles suggesting that even larger aggregates formed inside the guts. This effect was thought to be due to the reduced surface area as the powders agglomerated to microscale particles in solution and inside the guts. After 48 hours of exposure the nauplii eliminated the MoS₂ nanopowders as displayed by Fig. 11d.

No mortality was found neither in control group nor in the exposed organisms. The percentages of immobilized nauplii are reported in Table 2. The death % is not significant for both tested nanopowders.

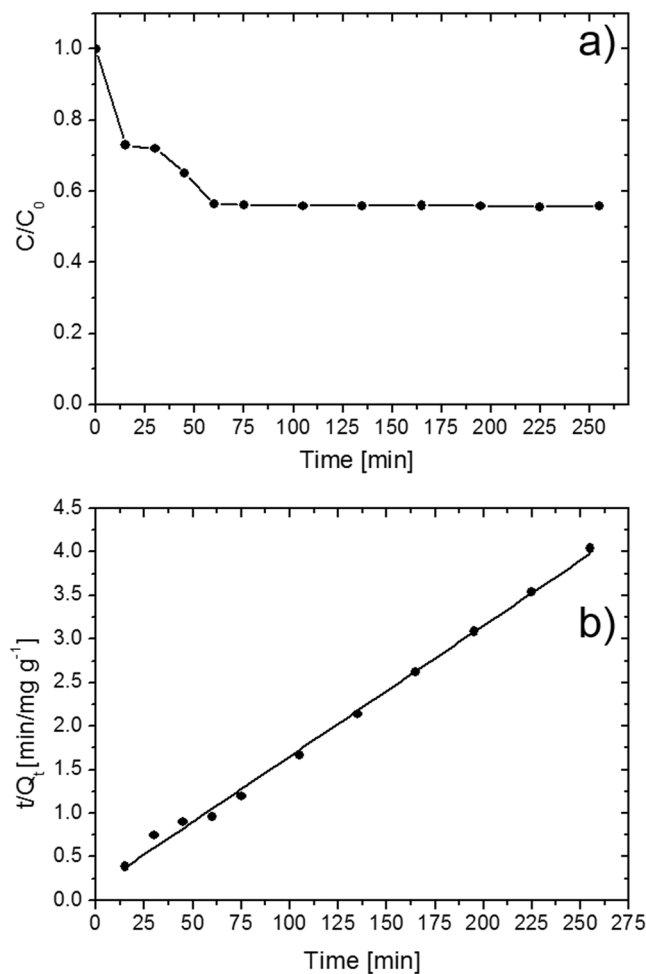


Figure 9. Phenol adsorption onto the ball-milled MoS₂ for 40 hours (a) (the line is guide for eye); adsorption kinetic of phenol onto the ball-milled MoS₂ for 40 hours compared with the pseudo-second-order model (b).

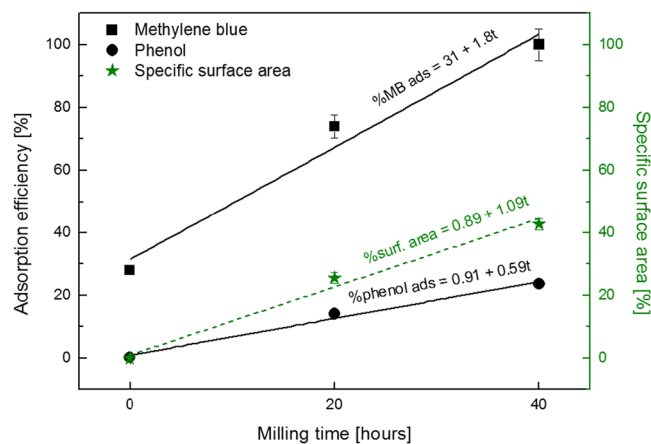


Figure 10. Efficiency of MB (black squares) and phenol (black circles) adsorption, and specific surface area increment of the samples (green stars) plotted as a function of the milling time. Black solid lines are the linear fits for MB and phenol adsorption efficiency, respectively. Green dashed line is the linear fit for the specific surface area increment. For each linear fit, the corresponding equation is indicated.

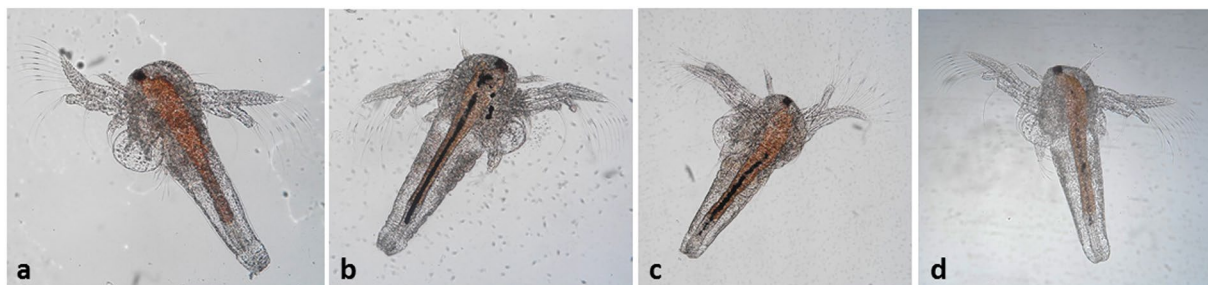


Figure 11. *Artemia salina* larvae: control at 24 hours (a), larve exposed to as received MoS₂ at 24 hours (b), larve exposed to ball-milled MoS₂ for 40 hours at 24 hours (c); larve exposed to ball-milled MoS₂ nanopowders at 48 hours, in which is evident the reduction of the gut contents (d).

	10 ⁻¹		10 ⁻²	
	24 h	48 h	24 h	48 h
As received MoS ₂	1%	0%	0%	0%
Ball milled MoS ₂ 40 h	1%	0%	0%	3%

Table 2. Percentages of immobilized nauplii after exposition to as received and ball milled MoS₂ at two different concentrations for both 24 and 48 hours.

Conclusions

Commercial MoS₂ nanopowders were processed by ball-milling for 20 or 40 hours. The milling process induced a significantly enhancement of the adsorption properties of MoS₂ nanopowders. In particular, in only 20 minutes the MoS₂ ball-milled for 40 hours was able to remove by adsorption 100% of MB dye initially presents in the aqueous solution. In addition, the adsorption capacity of MoS₂ towards phenol was steeply intensified by ball-milling. Thanks to an accurate characterization of the investigated materials, the improved performance of the ball-milled nanopowders was correlated to the increase of the specific surface area, induced by the ball-milling process. Importantly, the recyclability tests revealed that the MoS₂ nanopowders can be easily regenerated and reused without losing the adsorption capacity. The non-toxicity of the studied nanopowders was established by testing the effect of the material on microcrustacean *Artemia salina* in aquatic environment. The present original results demonstrate that the highly-scalable dry ball-milling process can be used for the preparation of highly-efficient adsorbents. This material can be fruitfully applied in wastewater treatment.

References

- Huang, X., Zeng, Z. & Zhang, H. Metal dichalcogenide nanosheets: preparation, properties and applications. *Chem. Soc. Rev.* **42**, 1934 (2013).
- Mak, K. F., Lee, C., Hone, J., Shan, J. & Heinz, T. F. Atomically thin MoS₂: a new direct-gap semiconductor. *Phys. Rev. Lett.* **105**, 136805 (2010).
- Song, I., Park, C. & Choi, H. C. Synthesis and properties of molybdenum disulphide: from bulk to atomic layers. *RSC Adv.* **5**, 7495 (2015).
- He, Z. & Que, W. Molybdenum disulfide nanomaterials: structures, properties, synthesis and recent progress on hydrogen evolution reaction. *Appl. Mat. Today* **3**, 23–56 (2016).
- Li, X. & Zhu, H. Two-dimensional MoS₂: properties, preparation, and applications. *J. Mater. Chem.* **1**, 33–44 (2015).
- Butler, S. Z. *et al.* Progress, challenges and opportunities in two-dimensional materials beyond graphene. *ACS Nano* **7**, 2898 (2013).
- Liu, C. *et al.* Rapid water disinfection using vertically aligned MoS₂ nanofilms and visible light. *Nat. Nanotechnol.* **11**, 1098–1104 (2016).
- Yin, W. *et al.* MoS₂-nanosheet-assisted coordination of metal ions with porphyrin for rapid detection and removal of cadmium ions in aqueous media. *ACS Appl. Mater. Interfaces* **9**, 21392–21370 (2017).
- Hirunpinyopas, W. *et al.* Desalination and nanofiltration through functionalized laminar MoS₂ membranes. *ACS Nano* **11**, 11082–11090 (2017).
- Shannon, M. A. *et al.* Science and technology for water purification in the coming decades. *Nature* **452**, 301–310 (2008).
- Dervin, S., Dionysiou, D. D. & Pillai, S. C. 2D nanostructures for water purification: graphene and beyond. *Nanoscale* **8**, 15115 (2016).
- Cantarella, M., Impellizzeri, G. & Privitera, V. Functional nanomaterials for water purification. *Riv. Nuovo Cimento* **40**, 595 (2017).
- Di Mauro, A. *et al.* Novel synthesis of ZnO/PMMA nanocomposites for photocatalytic applications. *Sci. Rep.* **7**, 40895 (2017).
- Di Mauro, A., Cantarella, M., Nicotra, G., Privitera, V. & Impellizzeri, G. Low temperature atomic layer deposition of ZnO: applications in photocatalysis. *Appl. Catal. B.* **196**, 68–76 (2016).
- Di Mauro, A., Fragalà, M. E., Privitera, V. & Impellizzeri, G. ZnO for application in photocatalysis: from thin films to nanostructures. *Mater. Sci. Semicond. Process.* **69**, 44–51 (2017).
- Scuderi, V. *et al.* *Appl. Catal. B.* Rapid synthesis of photoactive hydrogenated TiO₂ nanoplates. **183**, 328–334 (2016).
- Narayan, R. Use of nanomaterials in water purification. *Mater. Today* **13**, 44–46 (2010).
- Liu, S., Yu, J. & Jaroniec, M. Tunable photocatalytic selectivity of hollow TiO₂ microspheres composed of anatase polyhedral with exposed {001} facets. *J. Am. Chem. Soc.* **132**, 11914–11916 (2010).
- Tan, K. B. *et al.* Adsorption of dyes by nanomaterials: recent developments and adsorption mechanisms. *Sep. Purif. Technol.* **150**, 229–242 (2015).
- Marsh, H. & Rodriguez-Reinoso, F. *Production and Reference Material*, in: *Activated Carbon*. Elsevier Science Ltd, Oxford (2006)
- Heiranian, M., Farimani, A. B. & Aluru, N. R. Water desalination with a single-layer MoS₂ nanopore. *Nat. Commun.* **6**, 8616 (2015).

22. Sabarinathan, M. *et al.* Exfoliation of monodispersed MoS₂ layered nanostructures by a ligand-assisted hydrothermal approach for the realization of ultrafast degradation of an organic pollutant. *RSC Adv.* **6**, 109495–109505 (2016).
23. Quinn, M. D. J., Ho, N. H. & Notley, S. M. Aqueous dispersions of exfoliated molybdenum disulfide for use in visible-light photocatalysis. *ACS Appl. Mater. Interfaces* **5**, 12751–12756 (2013).
24. Meng, X., Li, Z., Zeng, H., Chen, J. & Zhang, Z. MoS₂ quantum dots-interspersed Bi₂WO₆ heterostructures for visible light-induced detoxification and disinfection. *Appl. Catal., B* **210**, 160–172 (2017).
25. Hu, K. H., Cai, Y. K. & Li, S. Photocatalytic degradation of methylene blue on MoS₂/TiO₂ nanocomposite. *Adv. Mat. Res.* **197**, 996–999 (2011).
26. Tacchini, I., Terrado, E., Anson, A. & Martinez, M. T. Preparation of a TiO₂-MoS₂ nanoparticle-based composite by solvothermal method with enhanced photoactivity for the degradation of organic molecules in water under UV Light. *Micro Nano Lett.* **6**, 932–936 (2011).
27. Tao, J., Chai, J., Gun, L., Pan, J. & Wang, S. Effect of interfacial coupling on photocatalytic performance of large scale MoS₂/TiO₂ hetero-thin films. *Appl. Phys. Lett.* **106**, 081602 (2015).
28. Xiang, Q., Yu, J. & Jaroniec, M. Synergetic effect of MoS₂ and graphene as cocatalysts for enhanced photocatalytic H₂ production activity of TiO₂ nanoparticles. *J. Am. Chem. Soc.* **134**, 6575–6578 (2012).
29. Ran, F., Liu, H., Wang, X. & Guo, Y. A novel molybdenum disulfide nanosheet self-assembled flower-like monolithic sorbent for solid-phase extraction with high efficiency and long service life. *J. Chromatogr. A* **1507**, 18–24 (2017).
30. Kyzas, G. Z. & Matis, K. A. Nanoadsorbents for pollutants removal: a review. *J. Mol. Liq.* **203**, 159–168 (2015).
31. Yagub, M. T., Sen, T. K., Afroze, S. & Ang, H. M. Dye and its removal from aqueous solution by adsorption: a review. *Adv. Colloid Interface Sci.* **209**, 172–184 (2014).
32. Massey, A. T., Gusain, R., Kumari, S. & Khatri, O. P. Hierarchical microspheres of MoS₂ nanosheets: efficient and regenerative adsorbent for removal of water-soluble dyes. *Ind. Eng. Chem. Res.* **55**, 7124–7131 (2016).
33. Chen, P., Liu, X., Jin, R., Nie, W. & Zhou, Y. Dye adsorption and photo-induced recycling of hydroxypropyl cellulose/molybdenum disulfide composite hydrogels. *Carbohydr. Polym.* **167**, 36–43 (2017).
34. Nagarajan, V. & Chandiramouli, R. Adsorption studies of alcohol molecules on monolayer MoS₂ nanosheet—a First-principles insights. *Appl. Surf. Sci.* **413**, 109–117 (2017).
35. Wang, X. *et al.* High supercapacitor and adsorption behaviors of flower-like MoS₂ nanostructures. *J. Mater. Chem. A* **2**, 15958 (2014).
36. Qiao, X. Q., Hu, F. C., Tian, F. Y., Hou, D. F. & Li, D. S. Equilibrium and kinetic studies on MB adsorption by ultrahigh 2D MoS₂ nanosheets. *RSC Adv.* **6**, 11631 (2016).
37. Song, H. J., You, S., Jia, X. H. & Yang, J. MoS₂ nanosheets decorated with magnetic Fe₃O₄ nanoparticles and their ultrafast adsorption for wastewater treatment. *Ceram. Int.* **41**, 13896 (2015).
38. Wang, F. *et al.* Fe₃O₄@SiO₂@CS-TETA functionalized graphene oxide for the adsorption of methylene blue (MB) and Cu(II). *Appl. Surf. Sci.* **420**, 970–981 (2017).
39. Guo, S., Xu, H., Zhang, F., Zhu, X. & Li, X. Preparation and adsorption properties of nano magnetite silica gel for methylene blue from aqueous solution. *Colloids Surf., A* **546**, 244–253 (2018).
40. Zhou, Q., Jiang, X., Guo, Y., Zhang, G. & Jiang, W. An ultra-high surface area mesoporous carbon prepared by novel MnO-templated method for highly effective adsorption of methylene blue. *Chemosphere* **201**, 519–529 (2018).
41. Huang, Q. *et al.* Marrying the mussel inspired chemistry and Kabachnik-Fields reaction for preparation of SiO₂ polymer composites and enhancement removal of methylene blue. *Appl. Surf. Sci.* **422**, 17–27 (2017).
42. Yang, Y. *et al.* PVBA-Uio-66 using a flexible PVBA with multi-coordination groups as mixed ligands and their super adsorption towards methylene blue. *Dalton Trans.* **47**, 6538 (2018).
43. Du, Z. *et al.* Facile one-pot fabrication of nano-Fe₃O₄/carboxyl-functionalized baker's yeast composites and their application in methylene blue dye adsorption. *Appl. Surf. Sci.* **392**, 312–320 (2017).
44. Wang, H. *et al.* Microwave-assisted synthesis of reduced graphene oxide/titania nanocomposites as an adsorbent for methylene blue adsorption. *Appl. Surf. Sci.* **360**, 840–848 (2016).
45. Wu, X. L., Shi, Y., Zhong, S., Lin, H. & Chen, J. R. Facile synthesis of Fe₃O₄-graphene@mesoporous SiO₂ nanocomposites for efficient removal of Methylene Blue. *Appl. Surf. Sci.* **378**, 80–86 (2016).
46. Song, Y., Duan, Y. & Zhou, L. Multi-carboxylic magnetic gel from hyperbranched polyglycerol formed by thiol-ene photopolymerization for efficient and selective adsorption of methylene blue and methyl violet dyes. *J. Colloid Interface Sci.* **529**, 139–149 (2018).
47. Delogu, F., Gorrasi, G. & Sorrentino, A. Fabrication of polymer nanocomposites via ball milling: present status and future perspectives. *Prog. Mater. Sci.* **86**, 75–126 (2017).
48. Krishnamoorthy, K., Pazhamalai, P., Veerasubramani, G. K. & Kim, S. J. Mechanically delaminated few layered MoS₂ nanosheets based high performance wire type solid-state symmetric supercapacitors. *J. Power Source* **321**, 112–119 (2016).
49. Li, H. *et al.* Novel dual-petal nanostructured WS₂@MoS₂ with enhanced photocatalytic performance and a comprehensive first-principles investigation. *J. Mater. Chem. A* **3**, 20225 (2015).
50. Xing, T. *et al.* Gas protection of two-dimensional nanomaterials from high-energy impacts. *Sci. Rep.* **6**, 35532 (2016).
51. Ambrosi, A., Chia, X., Sofer, Z. & Pumera, M. Enhancement of electrochemical and catalytic properties of MoS₂. *Electrochem. Commun.* **54**, 36–40 (2015).
52. Xu, R. C., Xia, X. H., Wang, X. L., Xia, Y. & Tu, J. P. Tailored Li₂S-P₂S₅ glass-ceramic electrolyte by MoS₂ doping, possessing high ionic conductivity for all-solid-state lithium-sulfur batteries. *J. Mater. Chem. A* **5**, 2829 (2017).
53. Zhang, W. L. *et al.* Growth of polyaniline nanoneedles on MoS₂ nanosheets, tunable electroresponse, and electromagnetic wave attenuation analysis. *J. Phys. Chem. C* **121**, 4989–4998 (2017).
54. *Compendium of chemical terminology*, in: A. D. McNaught, A. Wilkinson (Eds.), The Gold Book, 2nd edn, Blackwell Scientific Publications, Oxford (1997)
55. Scuderi, M., Strano, V., Spinella, C., Nicotra, G. & Mirabella, S. Low-cost synthesis of pure ZnO nanowalls showing three-fold symmetry. *Nanotechnology* **29**, 135707 (2018).
56. Wyckoff, R. W. G.; *Crystal Structures*, Vol. 2. 2nd Edition, John Wiley & Sons, Inc., New York, London, Sydney (1964).
57. Petkov, V. *et al.* Structure of nanocrystalline materials using atomic pair distribution function analysis: study of LiMoS₂. *Phys. Rev. B* **65**, 092105 (2002).
58. Chao, Y. *et al.* Application of graphene-like layered molybdenum disulfide and its excellent adsorption behavior for doxycycline antibiotic. *Chem. Eng. J.* **243**, 60–67 (2014).
59. Liu, H. *et al.* Highly ordered mesoporous MoS₂ with expanded spacing of the (002) crystal plane for ultrafast lithium ion storage. *Adv. Energy Mater.* **2**, 970–975 (2012).
60. Su, H., Li, W., Han, Y. & Liu, N. Magnetic carboxyl functional nanoporous polymer: synthesis, characterization and its application for methylene blue adsorption. *Sci. Rep.* **8**, 6506 (2018).
61. Liu, J., Li, E., You, X., Hu, C. & Huang, Q. Adsorption of methylene blue on an agro-aste oiltea shell with and without fungal treatment. *Sci. Rep.* **6**, 38450 (2016).
62. Zhu, B., Xia, P., Ho, W. & Yu, J. Isoelectric point and adsorption activity of porous g-C₃N₄. *Appl. Surf. Sci.* **344**, 188–195 (2015).
63. Ma, D., Zhu, B., Cao, B., Wang, J. & Zhang, J. Fabrication of the novel hydrogel based on waste corn stalk for removal of methylene blue dye from aqueous solution. *Appl. Surf. Sci.* **422**, 944–952 (2017).

64. Song, H. J., You, S. & Jia, X. H. Synthesis of fungus-like MoS₂ nanosheets with ultrafast adsorption capacities toward organic dyes. *Appl. Phys. A* **121**, 541–548 (2015).
65. Chang, Y. P., Ren, C. L., Qu, J. C. & Chen, X. G. Preparation and characterization of Fe₃O₄/graphene nanocomposite and investigation of its adsorption performance for aniline and p-chloroaniline. *Appl. Surf. Sci.* **261**, 504–509 (2012).
66. Bonilla-Petriciolet, A. *et al.* (eds) Adsorption processes for water treatment and purification. Springer International Publishing AG 2017, <https://doi.org/10.1007/978-3-319-58136-1>.
67. Grabowska, E., Reszczńska, J. & Zaleska, A. Mechanism of phenol photodegradation in the presence of pure and modified-TiO₂: a review. *Water Res.* **46**, 5453–5471 (2012).
68. Zhu, X., Chang, Y. & Chen, Y. Toxicity and bioaccumulation of TiO₂ nanoparticle aggregates in daphnia magna. *Chemosphere* **78**, 209–215 (2010).

Acknowledgements

The authors wish to thank Dr. Giovanna Pellegrino (CNR-IMM) who performed XPS measurements, Dr. Sabrina Carroccio (CNR-IMM) for fruitful discussion, Giuseppe Pantè (CNR-IMM) and Carmelo Percolla (CNR-IMM) for the technical assistance.

Author Contributions

M.C. conceived the experiment, performed SEM analyses, the adsorption tests, interpreted data and wrote the paper, G.G. prepared the samples through ball-milling process, A.D.M. performed XRD measurements and interpreted XPS analyses, M.S. and G.N. performed and interpreted the TEM analyses, R.F. and S.S. performed and interpreted the N₂ adsorption-desorption measurements, M.E.S. and M.V.B. performed and interpreted the toxicity tests, V.P. supervised experiment, G.I. supervised the whole experiment and interpreted data. All authors reviewed the manuscript.

Additional Information

Competing Interests: The authors declare no competing interests.

Publisher's note: Springer Nature remains neutral with regard to jurisdictional claims in published maps and institutional affiliations.



Open Access This article is licensed under a Creative Commons Attribution 4.0 International License, which permits use, sharing, adaptation, distribution and reproduction in any medium or format, as long as you give appropriate credit to the original author(s) and the source, provide a link to the Creative Commons license, and indicate if changes were made. The images or other third party material in this article are included in the article's Creative Commons license, unless indicated otherwise in a credit line to the material. If material is not included in the article's Creative Commons license and your intended use is not permitted by statutory regulation or exceeds the permitted use, you will need to obtain permission directly from the copyright holder. To view a copy of this license, visit <http://creativecommons.org/licenses/by/4.0/>.

© The Author(s) 2019